

# Intergranular Crack Nucleation in Bicrystalline Materials Under Fatigue

H. M. Shodja

Department of Civil Engineering,  
Northwestern University,  
Evanston, IL 60208  
Assoc. Mem. ASME

Y. Hirose

Department of Material Science  
and Engineering,  
Kanazawa University,  
Kanazawa, Japan

T. Mura

Department of Civil Engineering,  
Northwestern University,  
Evanston, IL 60208  
Fellow ASME

*During cyclic deformation of polycrystalline materials, as substantiated by many experimental observations, due to existence of high stress concentration at the interfaces the preferential site of crack nucleation is intercrystalline. Accordingly, it is assumed that the highly localized cyclic deformation persistent slip band (PSB) occurs along the grain boundary (GB) which results in intergranular crack initiation. In the present work the irreversible accumulation of dislocations are used to characterize PSB by means of double pile-up which are composed of vacancy and interstitial dipoles. We shall give the mechanism and a quantitative remedy of ratcheting of plastic deformation peculiar to fatigue deformation. In a manner conceptually analogous to Griffith theory (1921), the critical number of cycles to failure and hence the S-N curves for crack initiation is obtained by considering the free energy of the system. The Gibbs free energy change  $\Delta G$  increases with the fatigue cycle number due to cyclic increment of elastic strain energy which in turn stems from cyclic pile-up of dislocations along the slip planes. The Gibbs free energy change attains its maximum value at a critical cycle number beyond which the state of dislocation dipole accumulation becomes energetically unstable. In our theory we postulate that this critical state is the onset of crack initiation. We shall give a quantitative value for the fatigue limit and analyze the dependence of the S-N curve on several important physical parameters such as grain size; surface energy; yield strength; width of the PSB; and the ratio of the shear modulus of the bicrystalline material.*

## 1 Introduction

Deformation of bicrystalline materials is greatly affected by the presence of grain boundaries (GBs). To date, many experimental observations have confirmed that surfaces and interfaces such as GBs and twin boundaries are common sites for crack initiation. Westwood (1961) and Johnston et al. (1962), in their experimental studies reported the role of the GB in Magnesium Oxide bicrystals under compression. Johnston et al. studied the behavior of bicrystals with wide range of misorientations in some details. In this paper, we shall consider, as an element of a bicrystalline material two perfectly bonded crystals with compatible GB that are free of any microscopic inhomogeneities such as impurities and voids. Figure 1 depicts two situations where crystals A and B are the constituents of bicrystalline materials. In Fig. 1(b), crystal A is totally surrounded by crystal B.

Forsyth (1953) was the first to predict and observe extrusion phenomena in the fatigue of aluminium-copper alloy. Later, as pointed out in the review articles of Grosskreutz (1971), Laird and Duquette (1972), and the references therein, the extrusion phenomena was also observed in a wide variety of materials including most of the f.c.c, b.c.c, and some h.c.p metals. The mechanism of crack nucleation, particularly under low strain amplitude fatigue, is primarily due to extrusion and intrusion from striations in grains adjacent to the free surface. Subsequently, this mechanism roughens the free surface, which are stress raisers on the surface and hence lead to crack initiation. Among other types of crack nucleation we should mention the

Zener-Stroh crack, which occurs in coalescence of edge dislocations in a pile-up against an obstacle such as a GB. However, the latter is not commonly observed during fatigue experimentation. Fatigue processes is usually accompanied by narrow bands of highly localized cyclic strain, namely persistent slip bands (PSBs). In contrast to the Zener-Stroh crack, numerous experimental observations reveal that, for most materials, formation of cracks at GBs is the consequence of pile-up and coalescence of edge dislocation on two closely spaced layers with a band width much smaller than the length of the layer. This is a manifestation of existence of high tensile stress over a small area between the slip planes. Note that under fatigue, the material within the band becomes soft compared to the matrix and subsequent cyclic loading causes an accumulation of damage or equivalent ratcheting of plastic deformation inside the PSBs.

The preferred site of crack nucleation in bicrystalline materials, particularly under high strain amplitude fatigue, is intergranular or transgranular crack initiation at the GB. This is due to the high resolved shear stress concentration which exists there. At elevated temperatures, GBs serve as a crack nucleus, regardless of strain amplitude. At high plastic strain amplitude,  $\Delta\epsilon_{pl}$ , and high cyclic plastic strain rate,  $\dot{\epsilon}_{pl}$ , Mughrabi et al. (1981) attributed the nonoccurrence of fatigue cracks in slip bands and the preferential intercrystalline crack initiation in polycrystalline  $\alpha$ -iron to incompatible shape changes resulting from asymmetric slip in neighboring grains at the surface. On the other hand, under the same  $\Delta\epsilon_{pl}$  but low  $\dot{\epsilon}_{pl}$ , the slip bands become more prominent and the mode of crack nucleation is predominantly transgranular (Mughrabi, 1975; Mughrabi et al., 1981). Nevertheless, in our theoretical model we shall assume that, the formation of PSB along the GB eventually leads to intercrystalline crack initiation. The dislocation dipole model has been used to simulate PSB and nucleation of microvoids at the interface between a thin film and a substrate (Mura, 1994; Qin et al. 1991). We shall use vacancy and interstitial dipoles to model PSBs. As illustrated in Figs. 2(a), (b), and (c) we predict

Contributed by the Applied Mechanics Division of THE AMERICAN SOCIETY OF MECHANICAL ENGINEERS for publication in the ASME JOURNAL OF APPLIED MECHANICS.

Discussion on this paper should be addressed to the Technical Editor, Professor Lewis T. Wheeler, Department of Mechanical Engineering, University of Houston, Houston, TX 77204-4792, and will be accepted until four months after final publication of the paper itself in the ASME JOURNAL OF APPLIED MECHANICS.

Manuscript received by the ASME Applied Mechanics Division, Dec. 9, 1994; final revision, Aug. 1, 1995. Associate Technical Editor: D. M. Barnett.

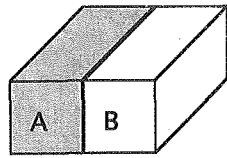


Fig. 1(a)

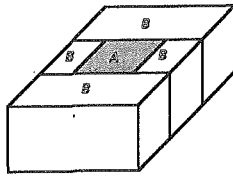


Fig. 1(b)

Fig. 1 Two examples of bicrystalline materials

three distinct possibilities for the formation of PSB with respect to the interface, with points  $O$  and  $O'$  indicating the internal dislocation sources, such as the Frank-Reed type source. Figure 3 shows the applied cyclic loading with  $\tau_{\max}$  and  $\tau_{\min}$  as the maximum and minimum shear stresses, respectively, with loading amplitude,  $\Delta\tau = \tau_{\max} - \tau_{\min}$ . We assume that, before loading, the crystals are free of any dislocations. When first loading to point 1, as shown in Fig. 3, the source  $O$  is activated emitting dislocation pairs of positive and negative signs along layer  $I$ . Similarly upon reversal of loading to point 2, the internal source  $O'$  emits dislocation pairs of both signs along layer  $II$ . The presence of some strong obstacles on either side of the internal sources in the path of layers  $I$  and  $II$  allow for the double pile-up of dislocations against the obstacles along these layers. Continued cyclic loading increases the dislocation density in the pile-up. Consequently, high density of vacancy dipoles at one end and high density of interstitial dipoles at the other end is equivalent to the movement of the material from the high density region of vacancy dipoles across  $OO'$  toward the high density region of interstitial dipoles. Eventually, this process results in microvoid nucleation in the region with a high density of vacancy dipoles, and hillock formation in the region of high interstitial dipoles.

The criteria used for obtaining the critical cycle number for fatigue life and subsequently obtaining the  $S-N$  ( $S$ : applied stress amplitude,  $N$ : number of cycles to crack initiation) curve is adopted from Mura and Nakasone (1990) and is similar to Griffith theory (1921). The energy of a Griffith crack under a fixed applied stress continues to increase with crack length up to the (unstable) equilibrium crack length at which the total free energy attains its maximum. Similarly for the fatigue problem, for a given stress amplitude  $\Delta\tau$ , the Gibbs free-energy change  $\Delta G$  is expressed as a function of cycle number  $n$  (Fig. 4). This free energy change increases with the fatigue cycle number due to the increase in elastic strain energy and becomes maximum at a critical cycle number beyond which the initial state of dislocation dipole accumulation becomes energetically unstable. The energy of this state will be released by annihilation of dislocation dipoles of vacancy type followed by formation of intergranular fatigue crack. Using these concepts we shall analyze the effect of several important physical parameters such as grain size; surface energy; yield strength; width of the PSB; and the ratio of the shear modulus of the crystals on the fatigue life of the bicrystal and give the corresponding  $S-N$  curves. One of the important features of these  $S-N$  curves that we gain in applying our theory is the fatigue limit, which indicates the threshold stress amplitude, below which cracks cannot be nucleated regardless of the number of cycles.

## 2 Mathematical Formulation of Dislocation Dipole Model

**2.1 Equilibrium of Peach-Koehler Force and the Governing Integral Equation.** Consider two perfectly bonded semi-infinite domains to represent an element of a bicrystalline material with three distinct situations, where slip planes are parallel to the interface, as depicted in Fig. 2. In this paper we focus on the case shown in Fig. 2(a). The remaining cases can be treated in a similar fashion. The material under consideration is elastic-perfectly plastic, so that the frictional stress  $\tau_f$ , which is the stress necessary for moving a dislocation inside the crystal lattice is constant. At stage 1 of loading cycle (Fig. 3) the maximum applied shear stress  $\tau_{\max}$  is greater than  $\tau_f$  and hence results in dislocation distribution on layer  $I$ . At the onset of

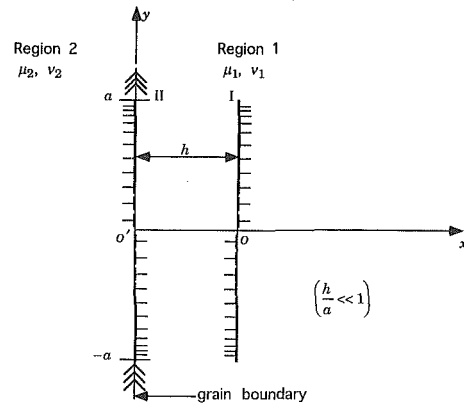


Fig. 2(a)

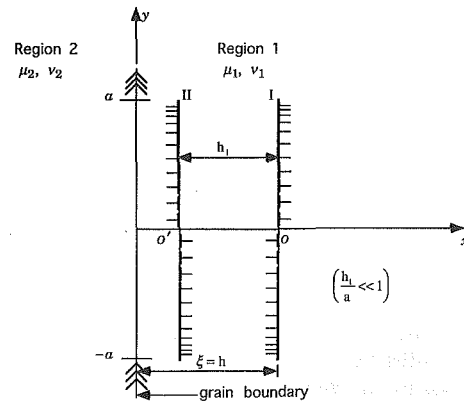


Fig. 2(b)

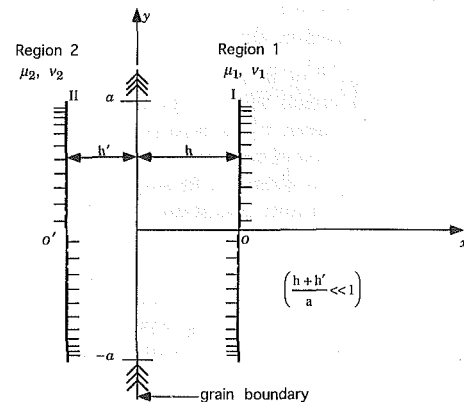


Fig. 2(c)

Fig. 2 Dislocation dipole model of the PSB at the GB, slip plane  $II$  is (a) at the GB (b) inside region 1 and (c) inside region 2

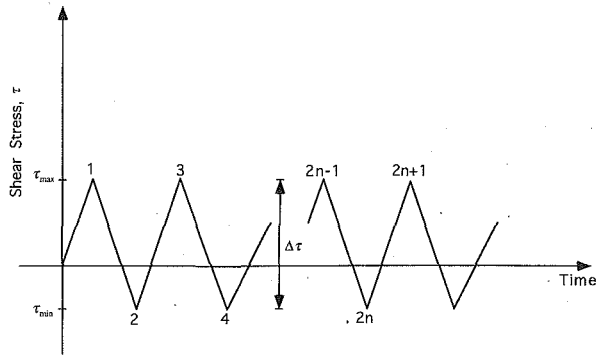


Fig. 3 Cyclic shear stress pattern acting on the slip planes versus time

plastic flow, the equilibrium of Peach-Koehler force on the piled-up dislocations along the slip plane *I* yields

$$\tau_1^D + \tau_{\max} = \tau_f, \quad (1)$$

where  $\tau_1^D$  is the back stress (dislocation stress) due to the dislocation distribution on layer *I* at stage 1 of the loading cycle. While the dislocation stress  $\tau_1^D$  is positive on layer *I*, it contributes a negative back stress, but nearly equal magnitude on layer *II*, which is located very close to layer *I*. The magnitude of the back stress  $\tau_1^D$  decreases with distance from layer *I*. Therefore, in view of the above and the assumption that dislocation motion is irreversible, it is reasonable that, upon unloading, the reverse slip occurs very close to layer *I*. On the other hand, in order to avoid annihilation of dislocations, the minimum distance between layers *I* and *II* must be of dislocation cell size. Ad hoc the distance between the two layers is negligible as compared to the length of the pile-up.

Load reversal to point 2 of the loading cycle, with the corresponding minimum applied shear stress  $\tau_{\min}$ , gives rise to the dislocation stress  $\tau_2^D$  due to new generation of dislocation distribution along layer *II*. The equilibrium of Peach-Koehler force on the piled-up dislocation along the newly formed slip plane *II* is given by

$$\tau_2^D + \tau_1^D + \tau_{\min} = -\tau_f. \quad (2)$$

As it appears from Eq. (2), the reverse plastic flow on layer *II* is indeed assisted by the back stress  $\tau_1^D$ . In this manner, ratcheting of plastic deformation is incorporated into our theoretical model. The mechanism of the build up of large local plastic strains with cyclic loading within two closely located thin slices was described by Lin and Ito (1969); however, their study did not consider dislocations, which play a fundamental role.

Combining Eqs. (1) and (2) and utilizing  $\Delta\tau = \tau_{\max} - \tau_{\min}$ ,

$$\tau_2^D = \Delta\tau - 2\tau_f. \quad (3)$$

It follows that at stage 2 of loading cycle,  $\Delta\tau$  must be greater than  $2\tau_f$  in order to create new dislocations along layer *II*. Noting that the back stress  $\tau_2^D$  is positive on layer *I*, we see how this aids the formation of new dislocation distribution along the layer with dislocation stress  $\tau_3^D$  at stage 3 of loading cycle and results in the equilibrium condition

$$\tau_3^D + \tau_{\max} + \tau_2^D = \tau_f. \quad (4)$$

Reversal of loading reactivates the dislocation source *O'*, emitting additional dislocation pairs along layer *II*. The equilibrium condition along layer *II* and at stage 4 of the loading cycle is

$$\tau_4^D + \tau_{\min} + \tau_3^D = -\tau_f, \quad (5)$$

where  $\tau_4^D$  is the back stress due to the dislocation distribution on layer *II*. At this point the trend of acceleration of the damage with each loading cycle is clearly seen from Eqs. (1), (2),

(4), and (5), in which the current applied back stress is the accumulation of all the previous ones. With the aid of Eqs. (1) and (3), Eq. (4) may be rewritten as

$$\tau_3^D - \tau_1^D = -(\Delta\tau - 2\tau_f). \quad (6)$$

Similarly, Eqs. (4) and (5) yield

$$\tau_4^D - \tau_2^D = \Delta\tau - 2\tau_f. \quad (7)$$

Following the above pattern, after *n* loading cycles, the equilibrium of the Peach-Koehler force on the piled-up dislocations yield

$$\tau_{2n+1}^D - \tau_{2n-1}^D = -(\Delta\tau - 2\tau_f), \quad \text{on layer } I, \quad x = h,$$

$$\tau_{2n}^D - \tau_{2n-2}^D = \Delta\tau - 2\tau_f, \quad \text{on layer } II, \quad x = 0.$$

However, for a large cycle number *n* of fatigue loading and unloading,  $\tau_1^D/n \rightarrow 0$ , so that

$$\tau_{2n+1}^D \approx -n(\Delta\tau - 2\tau_f), \quad \text{on layer } I, \quad x = h, \quad (8)$$

$$\tau_{2n}^D \approx n(\Delta\tau - 2\tau_f), \quad \text{on layer } II, \quad x = 0. \quad (9)$$

Equations (8) and (9) yield at once

$$\tau_{2n+1}^D(y) \approx -\tau_{2n}^D(y).$$

That is, after a large cycle number of fatigue, the dislocation stresses, and consequently the dislocation distribution densities on the two layers, are approximately equal, but are of opposite signs. Hence

$$D_{2n+1}(y) \approx -D_{2n}(y),$$

where the dislocation density distribution  $D_{2n+1}(y)$  on layer *I* is obtained from the following integral equation:

$$\int_{-a}^a D_{2n+1}(\eta) \tau_{xy}(h, y; h, \eta) d\eta = -n(\Delta\tau - 2\tau_f), \quad (10)$$

where  $\tau_{xy}(h, y; h, \eta)$  is the shear stress field at  $(h, y)$  due to an edge dislocation at  $(h, \eta)$ .  $\tau_{xy}$  is given in the following subsection.

## 2.2 Stress Field of an Edge Dislocation Near the Grain Boundary.

The problems of the interaction of dislocations and boundaries, and edge dislocations in inhomogeneous media were first studied by Head (1953a, b). Consider two perfectly bonded elastic half-spaces with shear moduli  $\mu_1, \mu_2$  and Pois-

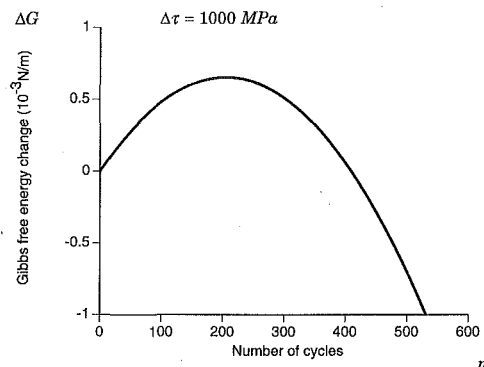


Fig. 4 Typical plot of Gibbs free-energy change versus cycle number. Critical cycle number occurs when  $\Delta G$  attains its maximum.

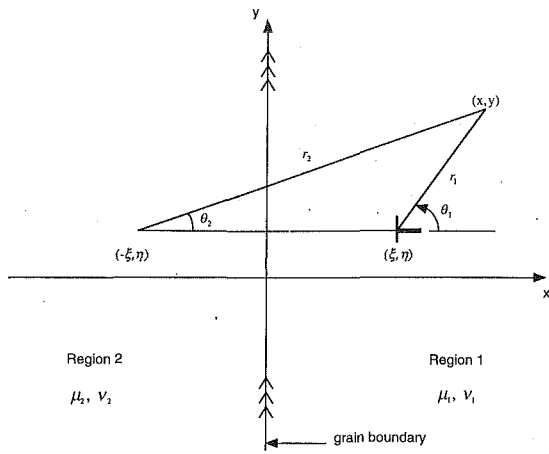


Fig. 5 An edge dislocation near an interface located at  $(\xi, \eta)$  in region 1

son's ratios  $\nu_1, \nu_2$ . As depicted in Fig. 5, a single edge dislocation is located at  $(\xi, \eta)$  in region 1 of the two joined half-spaces with its Burgers vector parallel to the interface. The coordinates and the geometrical location of the edge dislocation, with respect to its image at  $(-\xi, \eta)$  and the field point  $(x, y)$  are also shown in Fig. 5. When an edge dislocation is located at  $(\xi, 0)$  in region 1 with its Burgers vector parallel to the interface, the Airy stress functions for the two regions are given by (Dundurs, 1969)

$$\chi^{(1)} = \frac{2\mu_1 b_y}{\pi(\kappa_1 + 1)(1 - \beta^2)} \left\{ (1 - \beta^2)(r_1 \log r_1) \cos \theta_1 + (\alpha + \beta^2)(r_2 \log r_2) \cos \theta_2 - (1 + \alpha)\beta r_2 \theta_2 \sin \theta_2 - (\alpha - \beta)(1 - \beta) \times \xi \left( 2 \log r_2 - \cos 2\theta_2 + 2\xi \frac{\cos \theta_2}{r_2} \right) \right\}, \quad (11)$$

$$\chi^{(2)} = \frac{2\mu_1 b_y (1 + \alpha)}{\pi(\kappa_1 + 1)(1 - \beta^2)} \left\{ (r_1 \log r_1) \cos \theta_1 + \beta(r_1 \theta_1 \sin \theta_1 + 2\xi \log r_1) \right\}, \quad (12)$$

where  $b_y$  is the Burgers vector,  $\alpha$  and  $\beta$  are Dundurs constants

$$\alpha = \frac{\Gamma(\kappa_1 + 1) - (\kappa_2 + 1)}{\Gamma(\kappa_1 + 1) + \kappa_2 + 1},$$

$$\beta = \frac{\Gamma(\kappa_1 - 1) - (\kappa_2 - 1)}{\Gamma(\kappa_1 + 1) + \kappa_2 + 1},$$

with  $\Gamma = \mu_2/\mu_1$ ,  $\kappa_1 = 3 - 4\nu_1$  and  $\kappa_2 = 3 - 4\nu_2$ . Employing the Airy stress function given by Eq. (11) and noting that  $\tau_{xy}(x, y; \xi, \eta) = \tau_{xy}(x, y - \eta; \xi, 0)$  it follows that

$$\tau_{xy}(x, y; \xi, \eta) = \frac{2\mu_1 b_y}{\pi(\kappa_1 + 1)(1 - \beta^2)} \times \left\{ -(1 - \beta^2) \frac{\sin \theta_1 \cos 2\theta_1}{r_1} - (\alpha + \beta^2) \frac{\sin \theta_2 \cos 2\theta_2}{r_2} + 2\beta(1 + \alpha) \frac{\sin \theta_2 \cos^2 \theta_2}{r_2} - \xi(\alpha - \beta)(1 - \beta) \left( -\frac{2 \sin 2\theta_2}{r_2^2} - \frac{2 \sin 4\theta_2}{r_2^2} + \frac{4\xi \sin \theta_2 (4 \cos^2 \theta_2 - 1)}{r_2^3} \right) \right\}. \quad (13)$$

In Eq. (13),  $r_1, r_2, \theta_1$ , and  $\theta_2$  are redefined according to Fig. 5. Combination of Eqs. (10) and (13) yield

$$\frac{1}{\pi} \int_{-a}^a \frac{D_{2n+1}(\eta)}{\eta - y} d\eta - \frac{1}{\pi} \int_{-a}^a k(y, \eta) D_{2n+1}(\eta) d\eta = A, \quad (14)$$

with

$$A = \frac{n(\kappa_1 + 1)(\Delta\tau - 2\tau_f)}{2\mu_1 b_y}, \quad (15)$$

$$k(y, \eta) = -\frac{\alpha + \beta^2}{8h(1 - \beta^2)} \sin 4\theta_2 + \frac{\alpha + \beta}{4h(1 - \beta)} \cos^2 \theta_2 \sin 2\theta_2 + \frac{\alpha - \beta}{4h(1 + \beta)} \sin 4\theta_2 \cos^2 \theta_2, \quad (16)$$

where  $-a \leq (y, \eta) \leq a$ . The first term in Eq. (14) has a Cauchy-type singularity  $1/(y - \eta)$  and the asterisk (\*) on the upper left corner of the integral sign means that the integral exists in the sense of a Cauchy principal value only. Equation (14) is a Fredholm integral equation of the first kind, with a generalized Cauchy type kernel  $1/(y - \eta)$  and a bounded Fredholm kernel  $k(y, \eta)$  and is solved when subjected to the condition

$$\int_{-a}^a D_{2n+1}(\eta) d\eta = 0. \quad (17)$$

This additional condition assures the uniqueness of the solution, and states that the net Burgers vector of the dislocation density distribution on the slip planes equals to zero. Due to the singular behavior of the integral Eq. (14) and its complicated Fredholm kernel, an analytical solution of Eq. (14), when subjected to the constraint Eq. (17), is difficult to obtain. To circumvent this difficulty, and to preserve the nature of the power singularity of the dislocation density distribution, we employ a special numerical scheme which we describe in the following section.

### 3 Dislocation Density Distribution

The type of singular integral equation which we described in the previous section requires the use of an appropriate quadrature scheme. In particular, the Gauss-Jacobi integration technique, which has been extended by Erdogan and Gupta (1972), provides a powerful scheme suitable for the singular integral equations of the type developed herein. To employ this scheme, we shall make use of a proper transformations of variables  $y$  and  $\eta$ , such that the integration limits  $(-a, a)$  of Eqs. (14) and (17) are transformed to the normalized interval  $(-1, 1)$ . Subsequently, discretization of Eqs. (14) and (17) leads to the following system of linear algebraic equations in dislocation density distribution

$$\sum_{i=1}^m \frac{1}{m} \mathcal{D}(t'_i) \left[ \frac{1}{t'_i - t_j} + \pi \mathcal{K}(t'_i, t_j) \right] = A, \quad j = 1, 2, \dots, m - 1, \quad (18)$$

$$\sum_{i=1}^m \mathcal{D}(t'_i) = 0. \quad (19)$$

The right-hand side  $A$  and the function  $\mathcal{K}$  are Hölder continuous in  $-1 \leq (t', t) \leq 1$

$$\mathcal{K}(t', t) = -\frac{a}{\pi} k(t', t),$$

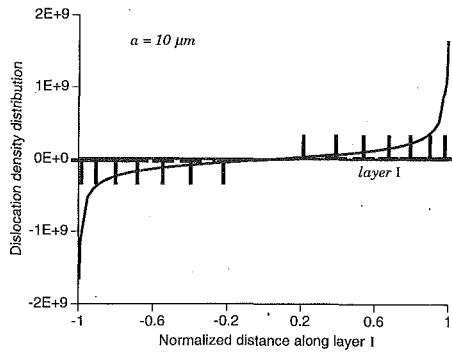


Fig. 6 Dislocation density distribution along the slip plane I

with  $\theta_2$  redefined as

$$\theta_2 = \tan^{-1} \frac{a(t-t')}{2h}$$

$\mathcal{D}(t')$  is a bounded function and is related to  $D_{2n+1}(t')$  through

$$\mathcal{D}(t') = \frac{D_{2n+1}(t')}{w(t')}$$

where the weight function  $w(t')$  has the same type of singularity at the end points of the interval  $-1 \leq t' \leq 1$  as  $D_{2n+1}(t')$  and is defined by

$$w(t') = \frac{1}{\sqrt{1-t'^2}}$$

Furthermore,

$$t'_i = \cos \frac{(2i-1)\pi}{2m}, \quad i = 1, 2, \dots, m,$$

$$t'_j = \cos \frac{j\pi}{m}, \quad j = 1, 2, \dots, m-1.$$

Figure 6 shows the graph of a typical dislocation density distribution along normalized distance on layer I, which was obtained for a pile-up with half-length equal to 10  $\mu\text{m}$ . As shown in Fig. 6, the dislocation density distribution is equal to zero at the center of the slip plane and varies gradually away from it; near the tips of the slip plane, however, it varies rather abruptly and eventually becomes infinite right at the tips.

#### 4 Gibbs Free-Energy Change and the S-N curves

The increase in Gibbs free-energy change  $\Delta G$  with the fatigue cycle number is due to cyclic increments of elastic strain energy, which in turn stems from cyclic pile-up of dislocations along the slip planes. The Gibbs free-energy change, from a state of dislocation dipole accumulation (Fig. 2(a)) to the state of crack initiation of size  $c$  (Fig. 7), is

$$\Delta G = -W_1 - W_2 + 2c\gamma_s, \quad (20)$$

where  $\gamma_s$  is the surface energy,  $W_1$  is the elastic strain energy release associated with the vacancy type dislocation dipoles, and  $W_2$  is the mechanical energy release due to the opening up of a crack embryo of size  $c$ . The stored energies  $W_1$  and  $W_2$  will be released when a crack is nucleated, while  $2c\gamma_s$  is the energy necessary to create the two faces of the microvoid of size  $c$

$$\begin{aligned} c &= b_y N(a) \\ &= b_y \int_0^a D_{2n+1}(\eta) d\eta, \end{aligned}$$

where  $N(a)$  is the total number of positive dislocations on layer I, equivalently in terms of the normalized variable introduced in previous section

$$c = ab_y \int_0^1 D_{2n+1}(t') dt'. \quad (21)$$

Since the mechanical energy release is much less than the elastic strain energy release, we shall discount  $W_2$ . The expression that relates elastic strain energy release to the self and interaction energies is given in the following subsection.

**4.1 Elastic Strain Energy; Relation to Interaction and Self Energies.** The stored elastic strain energy due to dislocation dipole accumulation may be written as

$$W_1 = \frac{1}{2} \int_{\Omega} \sigma_{ij}^D u_{i,j}^D dV, \quad (22)$$

where  $\sigma_{ij}^D$  and  $u_{i,j}^D$  are the dislocation stress and elastic distortion, respectively.  $dV$  is an elemental volume within the entire domain  $\Omega$ . When we employing the divergence theorem and note  $\sigma_{ij,j} = 0$  in  $\Omega$ , Eq. (22) becomes

$$W_1 = \frac{1}{2} \int_{\partial\Omega} \sigma_{ij}^D u_i^D n_j dS, \quad (23)$$

where  $dS$  is a surface element on the boundary  $\partial\Omega$  with outer unit normal  $n_j$ . Since the slip takes place only along layers I and II, with nonzero tractions, Eq. (23) yields

$$\begin{aligned} W_1 &= - \int_{-a}^a \tau_{2n+1}^D(h, y) [u_2^D(y)]_I dy \\ &\quad - \int_{-a}^a \tau_{2n+1}^D(0, y) [u_2^D(y)]_{II} dy, \quad (24) \end{aligned}$$

where  $\tau_{2n+1}^D(h, y)$  and  $\tau_{2n+1}^D(0, y)$  are the dislocation stresses caused by dislocation distribution along layer I. However,  $\tau_{2n+1}^D(h, y)$  is acting along layer I whereas  $\tau_{2n+1}^D(0, y)$  is acting on layer II. The slip distance  $[u_2^D(y)]_I$  at a point  $y$  on layer I is given by

$$\begin{aligned} [u_2^D(y)]_I &= (u_2^{D+}(y))_I - (u_2^{D-}(y))_I \\ &= b_y \{N(a) - N(|y|)\} \\ &= b_y \int_{|y|}^a D_{2n+1}(\eta) d\eta, \end{aligned}$$

for large enough cycle number  $n$  of fatigue loading and unloading the slip distance along layer II,  $[u_2^D(y)]_{II} \approx$

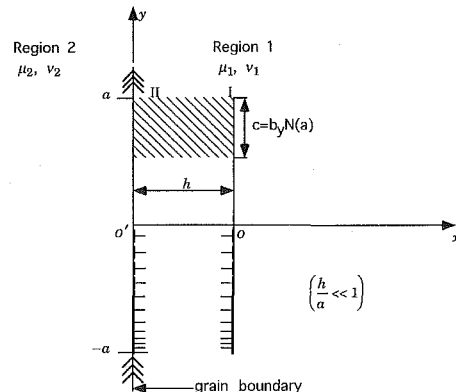


Fig. 7 Annihilation of dislocation dipoles of vacancy type followed by formation of intergranular crack embryo of size  $c$

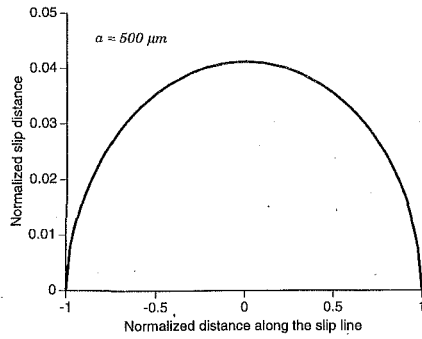


Fig. 8 Slip distance along the slip plane  $l$

$-[u_2^D(y)]_l$ . Using the transformation of variables which were introduced in Section 3

$$[u_2^D(t)]_l = ab_y \int_{|t|}^1 D_{2n+1}(t') dt' \quad (25)$$

Recall that dislocation density distribution is antisymmetric (Fig. 6), whereas in Fig. 8, the slip distance versus normalized distance along the slip plane is symmetric.

The first and second terms on the right-hand side of Eq. (24) are the self and the interaction energies, respectively. We denote the self energy by  $W_{\text{self}}$  and those of interaction energy by  $W_{\text{int}}$ , thus we may rewrite Eq. (24) as

$$W_1 = 2(W_{\text{self}} + W_{\text{int}}). \quad (26)$$

With the aid of the transformation of the variables introduced in Section 3, the self and interaction energies for layer  $l$  becomes

$$W_{\text{self}} = -\frac{1}{2} a \int_{-1}^1 \tau_{2n+1}^D(h, t) [u_2^D(t)]_l dt, \quad (27)$$

$$W_{\text{int}} = -\frac{1}{2} a \int_{-1}^1 \tau_{2n+1}^D(0, t) [u_2^D(t)]_{ll} dt. \quad (28)$$

Since  $[u_2^D]_{ll} \approx -[u_2^D]_l$  and  $\tau_{2n}^D \approx -\tau_{2n+1}^D$ , it turns out that  $W_{\text{self}}$  and  $W_{\text{int}}$  for layers  $l$  and  $ll$  are approximately equal, thus the factor 2 in Eq. (26) accounts for both layers.

**4.2 Crack Nucleation.** From Eqs. (18) and (19) we have

$$D_{2n+1}(t') = \mathcal{C}n(\Delta\tau - 2\tau_f)\Psi^{-1}(t', t)\Upsilon, \quad (29)$$

where  $\Psi_{m \times m}$  is the coefficient matrix,  $\Upsilon_{m \times 1} = \{1, 1, \dots, 1, 0\}^T$  and the constant  $\mathcal{C}$  contains some materials parameters. It follows that

$$\Delta G = c_1 n^2 (\Delta\tau - 2\tau_f)^2 + c_2 n (\Delta\tau - 2\tau_f) \gamma_s,$$

where the constants  $c_1$  and  $c_2$  contain information pertinent to material properties and geometry. The Gibbs free energy change  $\Delta G$  attains its maximum at a critical cycle number  $n_{cr}$ , beyond which the initial state of dislocation dipole accumulation becomes energetically unstable

$$n_{cr} = \frac{c_2 \gamma_s}{2c_1 (\Delta\tau - 2\tau_f)}, \quad (30)$$

hence the  $S$ - $N$  curves for fatigue crack initiation can be obtained. In plotting the  $S$ - $N$  curves,  $n_{cr} \equiv n_i$  determines the number of cycles to fatigue crack initiation. We assume that the embryonic crack of length  $c$ , which is created by the loading cycle number  $n_i$  becomes the unstable Griffith crack, which in turn extends to infinitely long crack, resulting in the fatigue failure. The plotting of Gibbs free-energy change  $\Delta G$  versus the number of cycles for different applied shear stress amplitudes are shown

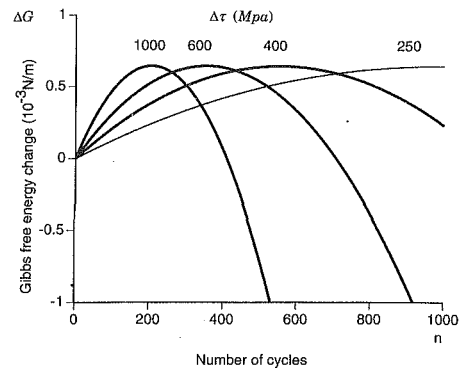


Fig. 9 Computed Gibbs free-energy change versus number of cycles for different applied shear stress amplitudes

in Fig. 9; we see that the critical cycle number increases with decreasing applied shear stress amplitude. The fact that the maximum Gibbs free energy change becomes less pronounced at lower applied shear stresses suggests a wider variation of fatigue life expectancy. It is interesting to note that the surface energy varies linearly with the critical cycle number, and has a square root dependence on the maximum Gibbs free-energy change.

## 5 Results and Discussion

According to the criteria set forth herein for obtaining the critical cycle number to fatigue life, we examine the effect of several important physical parameters on the  $S$ - $N$  curves. As it appears in Eq. (30), our theory predicts that the threshold stress amplitude (fatigue limit) below which cracks cannot be nucleated is twice the frictional stress for the dislocation motion. Since the failure mechanism is the one by slip along the PSBs, materials with higher frictional stress naturally exhibit a higher yield strength, which results in higher fatigue life, in agreement with our findings. The phenomenon of dependence of the  $S$ - $N$  curve on the frictional stress is illustrated in Fig. 10, where for a given  $\Delta\tau$ , we observe higher fatigue strength to crack initiation in the materials with higher  $\tau_f$ . In Fig. 10 the difference in the fatigue limits as the applied shear stress approaches  $2\tau_f$  is clearly demonstrated.

The effect of the surface energy on the  $S$ - $N$  curve is shown in Fig. 11, where an increase in  $\gamma_s$  results in higher fatigue resistance. As expected, the higher the surface energy the higher the number of cycles to failure and consequently higher energy is required for creation of two faces of a crack embryo, which further substantiates our theoretical results.

One of the important parameters considered in this study is the length of the slip plane which is representative of a grain size. From Fig. 12, we observe that materials with larger grain

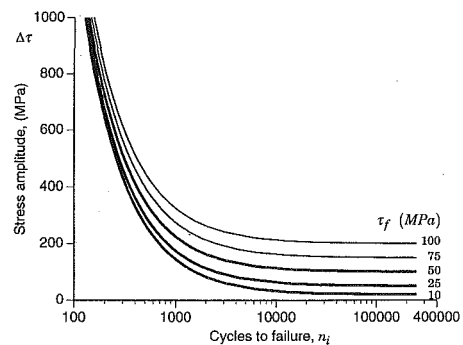


Fig. 10 Dependence of the  $S$ - $N$  curve and the corresponding fatigue limit on the frictional stress

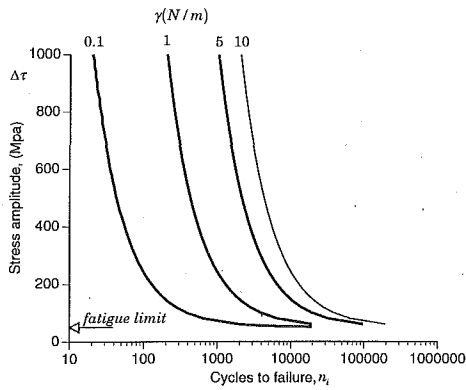


Fig. 11 Dependence of the S-N curve on the surface energy

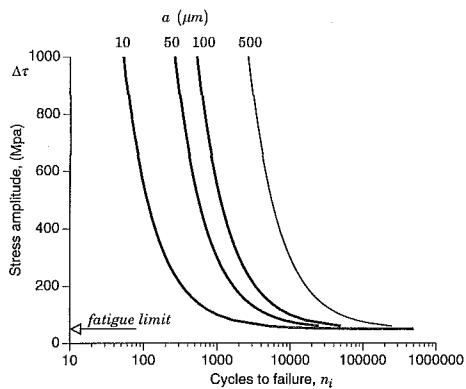


Fig. 12 Effect of the grain size on the fatigue life

size are stronger and have higher fatigue resistance. This is in agreement with experimental observations. Nakai et al. (1981) studied the effects of grain size on near-threshold fatigue crack propagation in low-carbon steel. The experimental results of Nakai et al., which is shown in Fig. 14, reveals that larger grain size materials correspond to higher threshold stress intensity range, and consequently have higher fatigue life. This phenomena was also confirmed by Gray et al. (1983). The microfractographic studies of fracture surfaces on the 7075 alloy in vacuum, which were performed by Petit (1983), indicate that the threshold fatigue crack growth rate is analogous to the fatigue crack initiation rate. This particular result of his experiment is shown in Fig. 15. Figure 13 depicts the solution of system of Eqs. (18) and (19) for the dislocation density distribution emitted from a single dislocation source for a fixed applied shear stress range

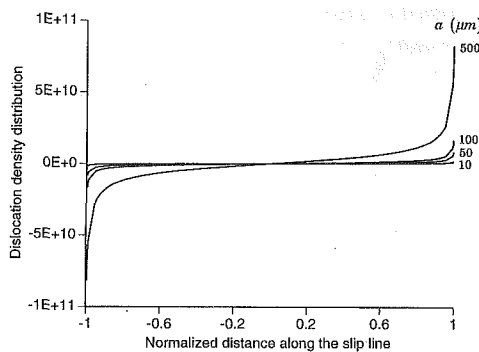


Fig. 13 Dislocation density distribution versus normalized distance along the slip plane. Dislocation pile-up shown for different half-length of slip planes correspond to the S-N curves shown in Fig. 12

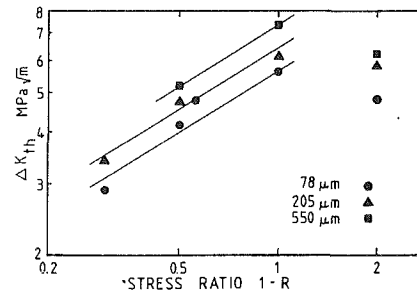


Fig. 14 Threshold stress intensity range,  $\Delta K_{th}$ , as a function of stress ratio,  $1-R$ , and effect of grain size in a low-carbon steel (Nakai et al., 1981)

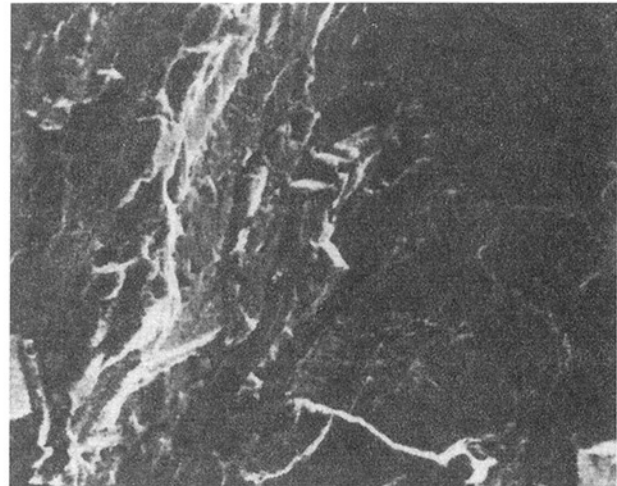


Fig. 15 Microfractographic view of fracture surface on the 7075 alloy in vacuum (Petit, 1983)

$\Delta\tau = 1$  Gpa and for slip planes of half length equal to 10, 50, 100, and 500  $\mu\text{m}$ , which correspond to the S-N curves shown in Fig. 12.

Under cyclic deformation, mutual annihilations of dislocations play an important role during glide. Essmann and Mughrabi (1979) studied the critical height of the dislocation dipoles of vacancy type of 1.6 nm for copper below which the annihilation of edge dislocations occurs. In weak beam TEM study of fatigued copper single crystals, Antonopoulos et al. (1976) reported edge-dislocation dipole widths from 2 to 5 nm with a mean of 3.5 nm. As depicted in Fig. 16, we considered a range of PSB widths  $h$  equal to 0.5, 1, 2.5 and 5 nm in order to demonstrate the qualitative effect of PSB width on the S-N

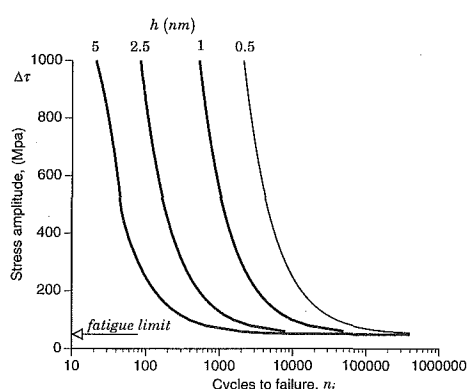


Fig. 16 Dependence of the S-N curve on the width of the PSB

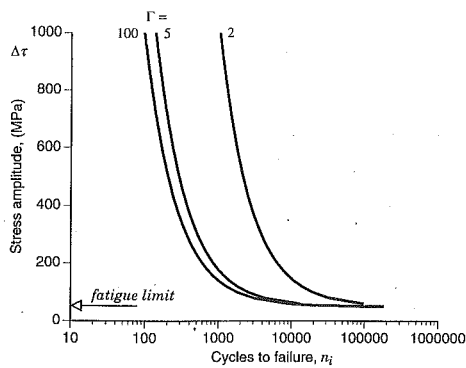


Fig. 17 Effect of ratio of the shear modulus of crystal 2 to those of crystal 1 ( $\Gamma = \mu_2/\mu_1$ ) on the fatigue life of the bicrystalline material

curves. We infer that, among the coexisting dislocation dipoles of various widths, which are shown in Fig. 16, for the largest band width  $h = 5$  nm it takes the least number of loading cycles to crack initiation.

The dependence of the  $S-N$  curves on the mismatch of the shear modulus is shown in Figs. 17; we conclude that larger mismatch of the shear modulus of grains results in lower fatigue resistance. In other words, we can say that the homogeneous materials have higher fatigue resistance to crack initiation. We close this section by noting that Figs. 11, 12, 16, and 17 were all obtained for the same value of friction stress  $\tau_f = 25$  Mpa; therefore the same fatigue limit of 50 Mpa prevails for these cases.

## 6 Conclusions

Based on the existing studies, we proposed a model for dislocation dipole pile-up peculiar to intergranular fatigue crack initiation in bicrystalline materials. The phenomena of ratcheting of plastic deformation within two closely located thin slices or equivalently within the so-called PSBs, and acceleration of the damage with each loading cycle, were incorporated in our theoretical formulation through consideration of back stress.

We have shown that the dislocation density distribution along the slip plane is minimal away from the tip of the pile-up and becomes infinite right at the tip. The maximum Gibbs free-energy change corresponds to a critical cycle number, beyond which crack initiates at the tip of the pile-up of vacancy dipoles. We thoroughly analyzed the effect of the grain size, surface energy, yield strength, width of the PSB and the ratio of the shear modulus of the bicrystalline material on its fatigue life and calculated the corresponding  $S-N$  curves. Finally, based on our theory presented herein, we were able to obtain the fatigue limit, an important feature of the  $S-N$  curves.

## Acknowledgments

This research was supported by AFOSR-F49620-92-J-0319.

## References

- Antonopoulos, J. G., Brown, L. M., and Winter, A. T., 1976, "Vacancy Dipoles in Fatigued Copper," *Philosophical Magazine*, Vol. 34, pp. 549–563.
- Dundurs, J., 1969, "Elastic Interaction of Dislocations with Inhomogeneities," *Mathematical Theory of Dislocations*, T. Mura, ed., pp. 70–115.
- Erdogan, F., and Gupta, G. D., 1972, "On the Numerical Solution of Singular Integral Equations," *Quarterly of Applied Mathematics*, Vol. 30, pp. 525–534.
- Essmann, U., and Mughrabi, H., 1979, "Annihilation of Dislocations During Tensile and Cyclic Deformation and Limits of Dislocation Densities," *Philosophical Magazine*, Vol. 40, pp. 731–756.
- Forsyth, P. J. E., 1953, "Exudation of Material from Slip Bands at the Surface of Fatigued Crystals of an Aluminum-Copper Alloy," *Nature*, Vol. 171, pp. 172–173.

Gray, III, G. T., Thompson, A. W., and Williams, J. C., 1983, "The Effect of Microstructure on Fatigue Crack Path and Crack Propagation Rate," *Fatigue Crack Growth Threshold Concepts*, D. Davidson and S. Suresh, eds., The Metallurgical Society of AIME, Oct. 3–5, pp. 131–143.

Griffith, A. A., 1921, "The Phenomena of Rupture and Flow in Solids," *Transactions of the Royal Society of London*, Vol. A221, pp. 163–179.

Grosskreutz, J. C., 1971, "The Mechanisms of Metal Fatigue," *Physica Status Solidi*, Vol. 47, pp. 359–396.

Head, A. K., 1953a, "The Interaction of Dislocations and Boundaries," *Philosophical Magazine*, Vol. 44, pp. 92–94.

Head, A. K., 1953b, "Edge Dislocations in Inhomogeneous Media," *The Proceedings of the Physical Society, London*, Vol. B66, pp. 793–801.

Johnston, T. L., Stokes, R. J., and Li, C. H., 1962, "Crack Nucleation in Magnesium Oxide Bi-crystals Under Compression," *Philosophical Magazine*, Vol. 7, pp. 23–34.

Laird, C., and Duquette, D. J., 1972, "Mechanisms of Fatigue Crack Nucleation," *Corrosion Fatigue*, O. F. Devereux, A. J. McEvily, and R. W. Staehle, eds., NACE 2, pp. 88–117.

Lin, T. H., and Ito, Y. M., 1969, "Mechanics of a Fatigue Crack Nucleation Mechanism," *Journal of the Mechanics and Physics of Solids*, Vol. 17, pp. 511–523.

Mughrabi, H., 1975, "Wechselverformung und Ermüdungsbruch von  $\alpha$ -Eisen-vielkristallen," *Zeitschrift für Metallkunde*, Vol. 66, pp. 719–724.

Mughrabi, H., Herz, K., and Stark, X., 1981, "Cyclic Deformation and Fatigue Behaviour of  $\alpha$ -Iron Mono- and Polycrystals," *International Journal of Fracture*, Vol. 17, pp. 193–220.

Mura, T., 1994, "A Theory of Fatigue Crack Initiation," *Materials Science and Engineering*, Vol. A176, pp. 61–70.

Mura, T., and Nakasone, Y., 1990, "A Theory of Fatigue Crack Initiation in Solids," *ASME JOURNAL OF APPLIED MECHANICS*, Vol. 57, pp. 1–6.

Nakai, Y., Tanaka, K., and Nakanishi, T., 1981, "The Effects of Stress Ratio and Grain Size on Near-Threshold Fatigue Crack Propagation in Low-Carbon Steel," *Engineering Fracture Mechanics*, Vol. 15, No. 3–4, pp. 291–302.

Petit, J., 1983, "Some Aspects of Near-Threshold Crack Growth: Microstructural and Environmental Effects," *Fatigue Crack Growth Threshold Concepts*, D. Davidson and S. Suresh, eds., The Metallurgical Society of AIME, Oct. 3–5, pp. 3–24.

Qin, S., Fan, H., and Mura, T., 1991, "Microvoid Nucleation at the Interface Between a Thin Film and a Substrate in Fatigue," *Journal of Applied Physics*, Vol. 70, pp. 1405–1411.

Westwood, A. R. C., 1961, "On the Fracture Behaviour of Magnesium Oxide Bi-crystals," *Philosophical Magazine*, Vol. 6, pp. 195–200.

## APPENDIX

In this appendix we shall give an alternative derivations of Eqs. (8) and (9). Consider the arbitrary stages  $2j - 2$ ,  $2j - 1$ ,  $2j$  and  $2j + 1$  of the loading cycles, then the corresponding equilibrium of Peach-Koehler force on the pile-up dislocations are

$$\tau_{2j-1}^D + \tau_{2j-2}^D + \tau_{\max} = \tau_f, \quad \text{on layer I, stage } 2j - 1, \quad (\text{A1})$$

$$\tau_{2j}^D + \tau_{2j-1}^D + \tau_{\min} = -\tau_f, \quad \text{on layer II, stage } 2j, \quad (\text{A2})$$

$$\tau_{2j+1}^D + \tau_{2j}^D + \tau_{\max} = \tau_f, \quad \text{on layer I, stage } 2j + 1, \quad (\text{A3})$$

from which we obtain

$$\tau_{2j}^D - \tau_{2j-2}^D = \Delta\tau - 2\tau_f, \quad (\text{A4})$$

$$\tau_{2j+1}^D - \tau_{2j-1}^D = -(\Delta\tau - 2\tau_f). \quad (\text{A5})$$

That is the net increment in the back stress between two consecutive even numbered stages (i.e., loading from  $\tau_{\min}$  to  $\tau_{\max}$  followed by unloading to  $\tau_{\min}$ ) and those of odd numbered stages (i.e., unloading from  $\tau_{\max}$  to  $\tau_{\min}$  followed by loading to  $\tau_{\max}$ ) are equal to  $\Delta\tau - 2\tau_f$  and  $-(\Delta\tau - 2\tau_f)$ , respectively. Hence, the net increments are invariant of the cycle number. In view of the above, it takes  $n$  increments for the even numbered stages to reach to stage  $2n$ , and starting from stage 1 it takes  $n$  increments for the odd numbered stages to reach to stage  $2n + 1$ . After large enough cycle number  $\tau_i^D$  will be negligible and we obtain

$$\tau_{2n+1}^D \approx -n(\Delta\tau - 2\tau_f), \quad \text{on layer I, stage } 2n + 1, \quad (\text{A6})$$

$$\tau_{2n}^D = n(\Delta\tau - 2\tau_f), \quad \text{on layer II, stage } 2n, \quad (\text{A7})$$

which are Eqs. (8) and (9) given in Subsection 2.1.